Enhancing Parathyroid Gland Visualization Using a Near Infrared Fluorescence-Based Overlay Imaging System

Melanie A McWade, PhD, Giju Thomas, PhD, John Q Nguyen, PhD, Melinda E Sanders, MD, Carmen C Solórzano, MD, FACS, Anita Mahadevan-Jansen, PhD

BACKGROUND: Misidentifying parathyroid glands (PGs) during thyroidectomies or parathyroidectomies could significantly increase postoperative morbidity. Imaging systems based on near infrared autofluorescence (NIRAF) detection can localize PGs with high accuracy. These devices, however, depict NIRAF images on remote display monitors, where images lack spatial context and comparability with actual surgical field of view. In this study, we designed an overlay tissue imaging system (OTIS) that detects tissue NIRAF and back-projects the collected signal as a visible image directly onto the surgical field of view instead of a display monitor, and tested its ability for enhancing parathyroid visualization.

STUDY DESIGN: The OTIS was first calibrated with a fluorescent ink grid and initially tested with parathyroid, thyroid, and lymph node tissues ex vivo. For in vivo measurements, the surgeon's opinion on tissue of interest was first ascertained. After the surgeon looked away, the OTIS back-projected visible green light directly onto the tissue of interest, only if the device detected relatively high NIRAF as observed in PGs. System accuracy was determined by correlating NIRAF projection with surgeon's visual confirmation for in situ PGs or histopathology report for excised PGs.

RESULTS: The OTIS yielded 100% accuracy when tested ex vivo with parathyroid, thyroid, and lymph node specimens. Subsequently, the device was evaluated in 30 patients who underwent thyroidectomy and/or parathyroidectomy. Ninety-seven percent of exposed tissue of interest was visualized correctly as PGs by the OTIS, without requiring display monitors or contrast agents.

CONCLUSIONS: Although OTIS holds novel potential for enhancing label-free parathyroid visualization directly within the surgical field of view, additional device optimization is required for eventual clinical use. (J Am Coll Surg 2019;228:730–743. © 2019 by the American College of Surgeons. Published by Elsevier Inc. All rights reserved.)

Inaccurate identification of parathyroid glands (PGs) during thyroidectomies, parathyroidectomies, or combined operations results in long-term postoperative implications for patients.[1-3] Accidental damage or excision of healthy PGs causes permanent hypocalcemia in about 12% of patients after thyroidectomies.[4] Conversely, 30% of parathyroidectomies required reoperation due to failure in removal of all diseased PGs.[5] Preoperative localization of diseased parathyroid glands are performed predominantly with sestamibi scintigraphy in conjunction with ultrasound

CME questions for this article available at http://jacscme.facs.org

Disclosure Information: Authors have nothing to disclose. Timothy J Eberlein, Editor-in-Chief, has nothing to disclose.

Support: This work was supported by the National Science Foundation Graduate Research Fellowship Program under NSF-0909667 (to McWade) and the NIH under grant nos. R41EB015291, R42CA192243, and 1R01CA212147-01A1 (to Mahadevan-Jansen).

Drs McWade and Thomas contributed equally to this work.

Received December 9, 2018; Revised January 24, 2019; Accepted January 29, 2019.

From the Vanderbilt Biophotonics Center, Department of Biomedical Engineering, Vanderbilt University (McWade, Thomas, Nguyen, Mahadevan-Jansen), Department of Pathology (Saunders), and Division of Surgical Oncology and Endocrine Surgery (Solórzano), Vanderbilt University Medical Center, Nashville, TN.

Correspondence address: Anita Mahadevan-Jansen, PhD, Department of Biomedical Engineering, Vanderbilt University, Station B, Box 351631, Nashville, TN 37235. email: anita.mahadevan-jansen@vanderbilt.edu

https://doi.org/10.1016/j.jamcollsurg.2019.01.017
ISSN 1072-7515/19

Abbreviations and Acronyms
FOV = field of view
NIRAF = near infrared autofluorescence
OR = operating room
OTIS = overlay tissue imaging system
PG = parathyroid gland

imaging, CT, or MRI.[6] Although sestamibi scintigraphy with ultrasound imaging has sensitivity ranging between 40% and 70%,[6-8] costs associated with CT or MRI scanning limit its routine use. Surgeons typically rely on visual inspection and surgical experience to identify PGs intraoperatively during head and neck surgical procedures. This can be problematic for resident trainees, low-volume center surgeons, and occasionally even for highly experienced surgeons.[9] As a result, surgeons tend to confirm the identity of parathyroid tissues using frozen-section analysis, which is, however, an invasive technique that adds to the time and costs of the surgical procedure. Intraoperative parathyroid hormone assay is another valuable technique that informs the surgeon if there is a need to explore for additional diseased (hypercellular) PGs after removing 1 diseased gland, thereby proving beneficial in confirming removal of all hyperactive PGs during parathyroidectomies.[10,11] However, this assay requires periodic blood sampling[12] and is rarely used during thyroidectomies. Because these techniques cannot be used to localize healthy PGs during thyroidectomies, there is a dire need for a reliable, real-time, noninvasive tool for identifying PGs, regardless of whether the glands are healthy or diseased, during all neck operations, including thyroidectomies and parathyroidectomies.

Our research group originally discovered near infrared autofluorescence (NIRAF) in PGs to be significantly elevated compared with adjacent neck tissues, after which we developed a noninvasive, label-free optical method using a hand-held surgical probe that performed point-based measurements for reliable parathyroid identification with 97% accuracy, irrespective of disease state.[13,14] The technology was then translated to a user-friendly clinical prototype "PTeye" that was recently FDA-approved for label-free parathyroid identification.[15,16] However, point-based measurements lacks the ability to provide spatial information regarding PGs. In contrast, an imaging system can acquire valuable spatial information and aid in visualizing PGs in context with adjacent anatomical structures. To address this need, we had earlier developed an imaging system that detects tissue with NIRAF, allowing the user to view the entire surgical field and localize PGs with 100% accuracy.[17] Since then, various groups have evaluated the potential of parathyroid localization using commercial NIR imaging systems, such as Fluobeam (Fluoptics) and Hamamatsu PDE systems (Hamamatsu Photonics).[18-22] However, when using intraoperative imaging modalities, including NIR imaging systems, it can be challenging to effectively correlate images seen on a display monitor with the anatomy observed directly under a surgeon's field of view (FOV), resulting in erroneous image interpretations.[23-25] In addition, staring at remote image displays and investing time for image output lessen the effectiveness of image-guided surgery.[26,27] These challenges could be offset by optimizing design ergonomics and image visualization techniques.[24,28]

Recent advances in improving intraoperative image visualization and co-registration involve virtually merging the acquired images with the actual surgical FOV. This merging has been investigated with microscope oculars, semi-transparent mirrors, or goggles worn by the surgeon.[29-31] A more intuitive approach would be to project the image directly onto the surgical FOV (see Fig. 1). Image projection onto skin is already used in commercial devices, such as VeinViewer and Accuvein, which relies on NIR light absorption by deoxygenated hemoglobin in the vein.[32] The concept of NIRAF-based image overlay was first demonstrated by Sarder and colleagues,[33] and was subsequently investigated in various animal models.[34,35] However, the motivation of those studies was restricted to tumor margin guidance and sentinel lymph node mapping, and depending heavily on exogenous contrast agent administration to boost NIRAF signal. Our group recently developed a modular NIRAF-based overlay tissue imaging system (OTIS) for wide-field intraoperative surgical guidance.[36] This portable device is designed to collect real-time optical images of the tissues, process the signal, and back-project a visible image directly onto the surgical FOV in real time, eliminating the need for a remote display monitor. In this article, we report on the capability of OTIS to enhance NIRAF visualization of PGs for the surgeon's naked eye directly in the surgical FOV without relying on remote display monitors or exogenous contrast agents in real time.

MATERIALS AND METHODS

Device description of overlay tissue imaging system

The OTIS comprises an NIR 785-nm diode laser (Innovative Photonics Solutions), an NIRAF image collection unit, a data processing laptop, and a visible light projection unit (Fig. 2A). The NIR diode laser was designed to illuminate a surgical FOV ranging from 5 × 5 cm (irradiance = 11.5 mW/cm^2) to 15 × 15 cm (irradiance = 0.6 mW/cm^2).

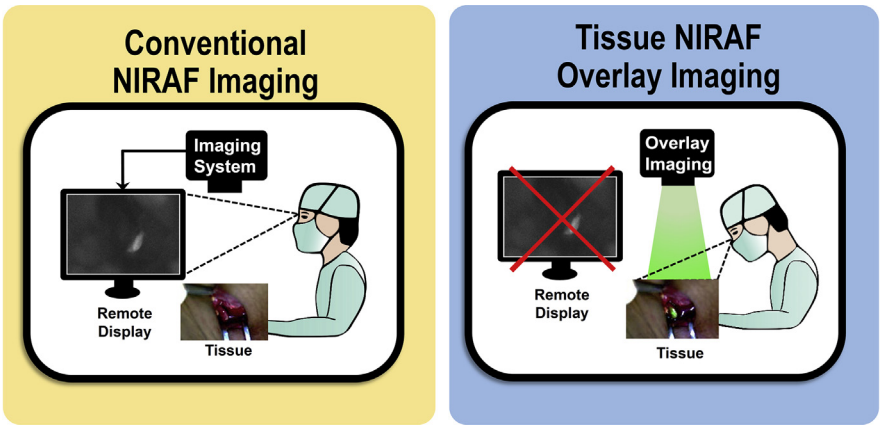

Figure 1. Comparison between conventional near infrared autofluorescence (NIRAF) imaging and tissue NIRAF overlay imaging. Conventional NIRAF images are typically displayed as gray-scale NIR images on a remote display that can lack comparability with the actual surgical site. Tissue NIRAF overlay imaging could provide the same information by image projection directly onto surgical site, offering improved spatial context. This also enables the surgeon's line of focus to stay in the surgical field without being diverted to a display monitor.

The NIRAF image collection unit consists of an NIR complementary metal oxide semiconductor camera (Basler AG) along with focusing optics and filters. The maximum spatial resolution for the NIRAF image collection unit in this system is 250 μm for a surgical FOV of 15 × 15 cm.[36] The visible light projection unit relies on a high-lumen light-emitting diode projector (AAXA Technologies). A color complementary metal oxide semiconductor camera (Basler AG) is additionally mounted for capturing images seen with the naked eye. The NIRAF image collection and visible light projection units are attached to a ball mount that can be positioned at any angle required

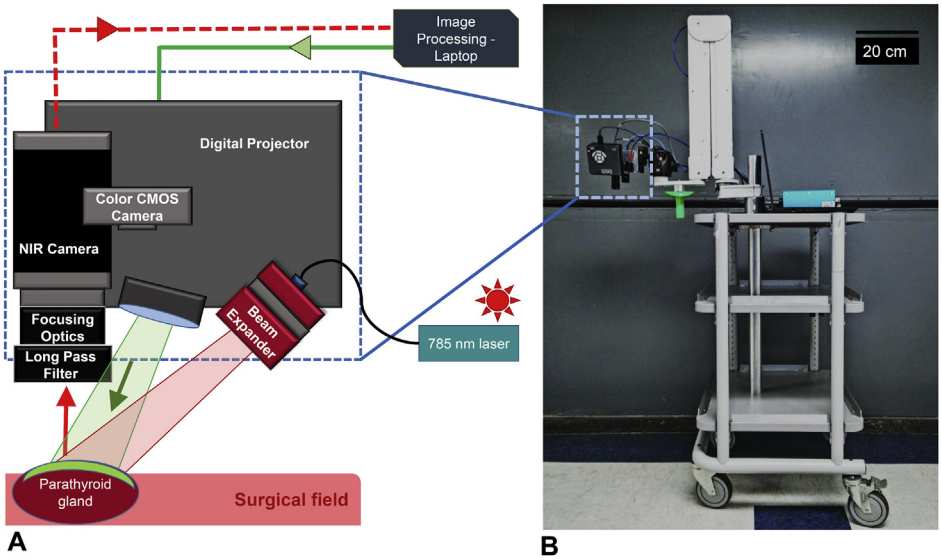

Figure 2. (A) Schematic of the imaging-projection unit of overlay tissue imaging system (OTIS). The unit comprises a 785-nm diode laser and a near infrared autofluorescence (NIRAF) image collection unit—a near infrared (NIR) camera with focusing and long pass filter optics, a data processing laptop, and a visible light projection unit. A color camera is additionally integrated to capture the projected image. (B) The imaging-projection unit is attached to ball mount, which in turn is connected to a double-articulated arm supported by a portable cart. A disposable sterile handle (green) is inserted into a slot designed on the arm, which permits the surgeon to conveniently position the imaging unit at any angle above the surgical field. CMOS, complementary metal oxide semiconductor.

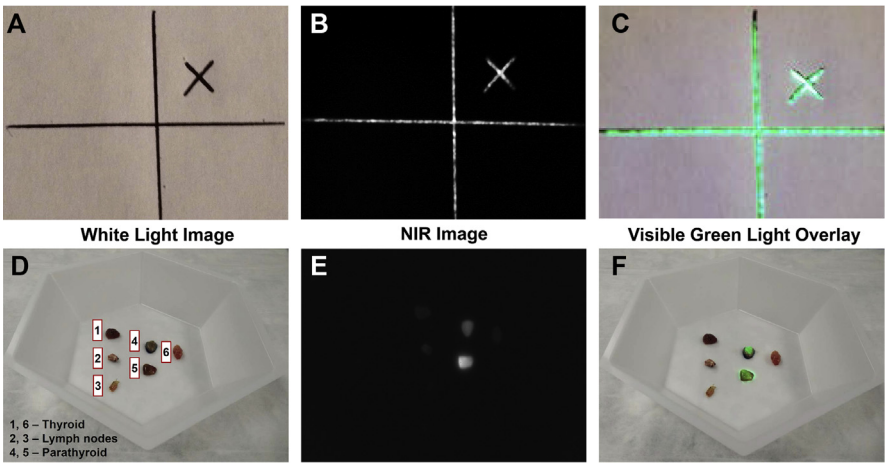

Figure 3. Ex vivo characterization and testing of overlay tissue imaging system (OTIS). (A) White light image of grid phantom sketched with near infrared (NIR) fluorescent ink. (B) An NIR image of the grid phantom. (C) Corresponding visible green light overlay onto the original target site indicating high spatial accuracy. (D) White light image of parathyroid adenoma, thyroid, and normal lymph node tissues. (E) The NIR image depicts relatively strong near infrared autofluorescence (NIRAF) signal from the 2 parathyroid adenomas only. (F) Visible green light is overlaid accurately over the 2 parathyroid adenoma specimens only, and thyroid and lymph node specimens received no green overlay.

(Fig. 2B). The mount is connected to a double-articulated arm attached to a portable cart that also holds the NIR laser and the laptop where image processing occurs through a user-interface designed with LabVIEW software (National Instruments).

Workflow with overlay tissue imaging system

For using OTIS, the surgeon first positions the imaging unit above the required FOV using a disposable sterile handle. After illuminating the required FOV with 785-nm diode laser, tissue fluorescence signal is detected by the camera in the NIRAF image collection unit. Raw NIRAF images are then relayed to the laptop for real-time processing using a customized algorithm in LabVIEW software. The algorithm first selects a user-defined region within the surgical FOV and then amplifies NIRAF signal by real-time feature extraction, and reduces ambient noise associated with stray operating room (OR) lights and background fluorescence.

After real-time feature extraction, the processed image is sent to the visible light projection unit and then converted here to a visible green intensity map, after which it is projected onto the surgical FOV. The visible light projection was performed only if NIRAF signal-to-background ratio was 1.5 or higher in the acquired NIR image. This threshold was set to ensure that visible light projection overlay was performed for parathyroid tissue only and not for nonparathyroid regions. The NIR camera and the projector unit are aligned such that the collected NIRAF image and projected visible image spatially overlap accurately. Images are continuously processed and projected onto the target FOV at a rate of 4 frames per second, allowing real-time, dynamic visualization of NIRAF information at the target site. The OTIS is designed with projection accuracy that lies within 0 to 1 mm,[36] which is well over the required resolution to aid in visualizing normal PGs (2- to 4-mm diameter).

Ex vivo validation of overlay tissue imaging system

Spatial accuracy of OTIS was first calibrated using a grid phantom sketched with NIR fluorescent ink on white paper (Fig. 3A). Alignment of the projected image with the actual sketched ink grid was evaluated for any spatial mismatch (Figs. 3B, 3C). Orientation of the NIRAF image collection and visible light projection unit were adjusted accordingly to minimize mismatch and ensure accurate co-registration of projected image with the sketched ink grid. This step was performed before each OTIS measurement to calibrate image alignment.

Frozen tissues obtained from the Vanderbilt Tissue Bank (Vanderbilt University Medical Center) comprising 2 specimens each of parathyroid adenomas, normal thyroid, and normal lymph nodes were first used for validating the ex vivo performance of OTIS. The frozen tissues were first thawed and then placed randomly on a nonreflective substrate at a distance of 35 cm below the OTIS. The NIRAF images were acquired with a 300-ms exposure time, and the entire workflow of NIRAF signal collection, image processing, and back-projection of visible green image took not

more than 2 minutes. The color complementary metal oxide semiconductor camera captured color images of tissues initially without, and later with, visible light overlay.

Intraoperative testing of overlay tissue imaging system

Thirty patients undergoing parathyroidectomy and/or thyroidectomy were recruited for this study at the Vanderbilt University Medical Center after approval from the IRB. Adult patients aged older than 18 years undergoing endocrine operation for thyroid and/or parathyroid disease were included in this study. Written informed consent was obtained from all enrolled patients before the procedure. Measurements were excluded from the study if no histology was available for the tissue of interest when identified with low confidence by the surgeon or if the OR lights were not turned completely off.

Before each procedure, image co-registration of the OTIS was evaluated using NIR fluorescent ink grid, as described earlier. For the purpose of parathyroid visualization with OTIS, an FOV measuring 5 × 5 cm was considered adequate, as surgical incision length for standard thyroidectomy and parathyroidectomy typically ranges between 4 and 6 cm.[37] Once the PGs were exposed, the confidence level (high, medium, or low) of the surgeon in visually identifying each PG was recorded. A visible white grid was first projected onto the surgical FOV to aid the surgeon in positioning the OTIS toward the region of interest. The surgeon then positioned OTIS approximately 35 cm above the surgical FOV using a disposable sterile handle (attached as seen in Fig. 2B), without affecting sterility of the surgical work flow. Subsequently all OR lights were turned off and surgical headlights were directed away to minimize light interference. The NIRAF images were collected, processed, and projected directly as visible images onto the surgical FOV as described in the previous section. The surgeon looked away and was blinded to the image projection of OTIS so as to not affect patient outcomes. Each in vivo measurement with OTIS took no more than 2 minutes, which included the entire process of capturing NIRAF image from region of interest and projecting it back as a visible color image directly onto the surgical site. Visual confirmation was used for identifying in situ healthy PGs during thyroidectomies, as these are not typically removed during operations, although frozen biopsy and histopathology reports were used for confirming identities of tissues excised during parathyroidectomies. Tissue sites with a low surgical confidence level were excluded from analysis, unless there was available histology from that tissue.

Statistical analysis

NIRAF signal was first normalized to the background signal to obtain NIRAF signal-to-background ratio and presented as mean ± SE. Two-tailed Student's *t*-tests for unequal variance were used to assess statistical significance, with values of $p < 0.05$ being considered significant.

RESULTS

The feasibility of real-time intraoperative OTIS to enhance parathyroid visualization was investigated in this study. The results demonstrate that NIRAF signal from PGs could be successfully projected as a visible image directly onto the surgical FOV with high accuracy, without requiring remote display monitors.

Ex vivo validation of overlay tissue imaging system

For the grid phantom sketched with NIR fluorescent ink (Fig. 3A), the OTIS first captured an NIRAF image of the inked grid (Fig. 3B) and then subsequently projected a visible green image (Fig. 3C) that was well-aligned spatially with the position of the grid phantom. When tested with tissue specimens ex vivo (Fig. 3D), OTIS achieved 100% accuracy in parathyroid identification—2 of 2 parathyroid tissues (100% sensitivity) and 4 of 4 nonparathyroid tissues—thyroid and lymph nodes (100% specificity). The NIRAF images captured by OTIS for tissue specimens indicated higher intensities for parathyroid adenoma specimens compared with the normal thyroid and lymph node tissues (Fig. 3E). Based on the detected NIRAF signal, OTIS projected visible green light on parathyroid specimens only and not on the nonparathyroid tissues, as seen in Figure 3F.

The projection overlay with OTIS is dynamic in nature—as the target (grid phantom or tissue specimens) shifts, the projected image overlay also shifts accordingly with high sensitivity. A demonstration of NIR fluorescence-based overlay imaging performed initially with a grid sketched with NIR fluorescent ink and subsequently with parathyroid, thyroid, and lymph node tissues ex vivo can be seen in Video 1. The delay or lag of the image overlay in relation to the target is less than 2 seconds.

Intraoperative testing of overlay tissue imaging system

For this study, 75 measurements were acquired with OTIS from regions of interest in 30 patients undergoing parathyroidectomy and/or thyroidectomy. Fifteen of these patients were diagnosed with hyperparathyroidism (primary or secondary), 12 patients had thyroid disease, and 3 patients had concurrent parathyroid-thyroid disease

Table 1. Overview of Patient Demographics, Diseases States, Tissue Histopathology, and Corresponding Intraoperative Assessment with Overlay Tissue Imaging System

Variable	Parathyroid histopathology	Surgeon confidence	Parathyroid in vivo NIRAF*	OTIS overlay
Thyroidectomy				
Benign thyroid goiter				
Patient number, age, sex, BMI				
No. 4, 55 y, F, 29.9 kg/m^2				
Surgeon opinion of parathyroid				
Healthy	NA	High	+	Y
Healthy	NA	High	+	Y
Healthy	NA	High	+	Y
Healthy	NA	High	++	Y
No. 8, 62 y, M, 25.2 kg/m^2				
Surgeon opinion of parathyroid				
Healthy	NA	High	++	Y
Healthy	NA	High	++	Y
No. 15, 59 y, F, 41.3 kg/m^2				
Surgeon opinion of parathyroid	NA	High	++	Y
Healthy				
No. 17, 58 y, F, 32.3 kg/m^2				
Surgeon opinion of parathyroid				
Healthy	NA	High	++	Y
Healthy	NA	High	++	Y
Healthy	NA	High	++	Y
No. 28, 50, F, 36.3 kg/m^2				
Surgeon opinion of parathyroid				
Healthy	NA	High	++	Y
Healthy	NA	High	+	Y
Graves' disease				
Patient number, age, sex, BMI				
No. 7, 51 y, F, 26.6 kg/m^2				
Surgeon opinion of parathyroid				
Healthy	NA	High	+	Y
Healthy	NA	High	+	Y
Healthy	NA	High	+	Y
Healthy	NA	High	+	Y
Papillary thyroid cancer				
Patient number, age, sex, BMI				
No. 3, 70 y, F, 28.5 kg/m^2				
Surgeon opinion of parathyroid				
Healthy	NA	High	++	Y
Healthy	NA	High	++	Y
No. 6, 32 y, F, 25.1 kg/m^2				
Surgeon opinion of parathyroid				
Healthy	NA	High	+	Y
Healthy	NA	High	+	Y
No. 10, 55 y, M, 26.6 kg/m^2				
Surgeon opinion of parathyroid				
Healthy	NA	High	++	Y
Healthy	NA	High	++	Y

(Continued)

Table 1. Continued

Variable	Parathyroid histopathology	Surgeon confidence	Parathyroid in vivo NIRAF*	OTIS overlay
No. 13, 59 y, F, 23.2 kg/m^2				
Surgeon opinion of parathyroid				
Healthy	NA	High	+	Y
Healthy	NA	High	+	Y
No. 20, 51, M, 32.2 kg/m^2				
Surgeon opinion of parathyroid				
Healthy	NA	High	+++	Y
No. 25, 29 y, F, 20.5 kg/m^2				
Surgeon opinion of parathyroid				
Healthy	NA	High	++	Y
Healthy	NA	High	-	N
Healthy	NA	High	++	Y
Healthy	NA	High	++	Y
Parathyroidectomy				
Primary hyperparathyroidism				
Patient number, age, sex, BMI				
No. 1, 66 y, F, 26.1 kg/m^2				
Surgeon opinion of parathyroid				
Healthy	NA	High	++	Y
Diseased	Hypercellular (adenoma)	High	++	Y
Healthy	NA	High	+++	Y
Diseased	Benign thyroid	Low	-	N
No. 9, 70 y, F, 22.8 kg/m^2				
Surgeon opinion of parathyroid				
Diseased	Hypercellular	High	++	Y
Diseased	Hypercellular	High	++	Y
Diseased	Hypercellular	High	++	Y
No. 12, 67 y, F, 47.8 kg/m^2				
Surgeon opinion of parathyroid				
Diseased	Hypercellular (adenoma)	High	++	Y
Healthy	NA	High	++	Y
No. 14, 39 y, F, 38.1 kg/m^2				
Surgeon opinion of parathyroid				
Diseased	Hypercellular	High	++	Y
Diseased	Normocellular	High	+++	Y
Diseased	Hypercellular	High	++	Y
No. 16, 64 y, F, 53.3 kg/m^2				
Surgeon opinion of parathyroid				
Healthy	NA	Moderate	+	Y
Healthy	NA	Moderate	++	Y
No. 18, 60 y, F, 38.1 kg/m^2				
Surgeon opinion of parathyroid				
Healthy	NA	High	++	Y
Healthy	NA	High	+++	Y
Diseased	Hypercellular (adenoma)	High	++	Y
No. 19, 61 y, M, 25.1 kg/m^2				
Surgeon opinion of parathyroid				
Diseased	Parathyroid carcinoma	High	-	N

(Continued)

Table 1. Continued

Variable	Parathyroid histopathology	Surgeon confidence	Parathyroid in vivo NIRAF*	OTIS overlay
No. 22, 52 y, F, 30.8 kg/m^2				
Surgeon opinion of parathyroid				
Diseased	Hypercellular (adenoma)	High	++	Y
Healthy	NA	High	+++	Y
No. 23, 74 y, F, 20.8 kg/m^2				
Surgeon opinion of parathyroid				
Diseased	Hypercellular	High	+	Y
Diseased	Hypercellular	High	++	Y
Diseased	Hypercellular	High	++	Y
No. 24, 43 y, M, 31 kg/m^2				
Surgeon opinion of parathyroid				
Diseased	Normocellular	Moderate	++	Y
Diseased	Hypercellular	High	+++	Y
No. 26, 55 y, F, 30.6 kg/m^2				
Surgeon opinion of parathyroid				
Diseased	Normocellular	High	++	Y
Healthy	NA	High	++	Y
Healthy	NA	High	++	Y
No. 27, 67 y, F, 32.1 kg/m^2				
Surgeon opinion of parathyroid				
Diseased	Hypercellular	High	++	Y
Diseased	Hypercellular	High	+++	Y
Healthy	NA	High	+	Y
Primary hyperparathyroidism (MEN-1)				
Patient number, age, sex, BMI				
No. 5, 57 y, M, 25.7 kg/m^2				
Surgeon opinion of parathyroid				
Diseased	Hypercellular	High	+++	Y
Diseased	Hypercellular	High	++	Y
Recurrent hyperparathyroidism				
Patient number, age, sex, BMI				
No. 21, 65 y, F, 25.2 kg/m^2				
Surgeon opinion of parathyroid				
Diseased	Hypercellular (adenoma)	High	++	Y
Secondary hyperparathyroidism				
Patient number, age, sex, BMI				
No. 11, 46 y, F, 36.8 kg/m^2				
Surgeon opinion of parathyroid				
Diseased	Hypercellular	High	++	Y
Diseased	Hypercellular	High	++	Y
Thyroidectomy combined with parathyroidectomy				
Primary hyperparathyroidism with benign thyroid goiter				
Patient number, age, sex, BMI				
No. 2, 73 y, F, 28 kg/m^2				
Surgeon opinion of parathyroid				
Diseased	Hypercellular (adenoma)	High	+++	Y

(Continued)

Table 1. Continued

Variable	Parathyroid histopathology	Surgeon confidence	Parathyroid in vivo NIRAF*	OTIS overlay
No. 29, 57 y, F, 26.2 kg/m^2				
Surgeon opinion of parathyroid				
Diseased	Hypercellular (adenoma)	High	++	Y
Healthy	NA	High	+++	Y
Healthy	NA	High	++	Y
No. 30, 35 y, F, 24.5 kg/m^2				
Surgeon opinion of parathyroid				
Diseased	Hypercellular (adenoma)	High	+	Y

*Signal-to-background ratio grading: −[<1.5]; + [1.5 to 2.2]; ++ [2.3 to 4.9]; +++ [>5].
MEN-1, multiple endocrine neoplasia type 1; N, no; NA, not applicable; NIRAF, near infrared autofluorescence; OTIS, overlay tissue imaging system; Y, yes.

(Table 1). Of the 75 measurements obtained with OTIS, 4 were excluded due to interference from OR lights that were not switched off completely. It must be emphasized that, as described earlier, the OR lights were meant to remain off during the measurements. However, in these 4 glands, the OR lights remained on accidentally, which interfered with NIRAF measurements from the tissue in view. The NIRAF signal from parathyroid could not be detected due to OR light interference, leading to exclusion of these measurements. In addition to those 4 glands, measurement from another gland was omitted due to system error, and the remaining 70 were eventually considered for further data analysis.

Figure 4 depicts OTIS images acquired from the surgical FOV of 4 patients, where the left column (Figs. 4A to 4D) display white light images similar to what is seen by the surgeon's naked eye (Figs. 4A to 4D) before NIRAF image capture with OTIS. The right column of images (Figs. 4E to 4H) shows white light images of the same surgical site in the corresponding patients after OTIS projects the NIRAF image onto the surgical FOV with visible green light. The overlay in green color provided enhanced visual contrast for PGs against adjacent tissue structures directly at the surgical site. It should be noted that intensity of the green overlay directly correlated with NIRAF signal intensity collected from the PGs. In this study, 45 healthy PGs had an averaged NIRAF signal-to-background ratio of 4.51 ± 1.24, which was not significantly different from that of 24 diseased PGs (adenomas, multiglandular hyperplasia, and carcinoma) of 4.81 ± 0.80. Adjacent neck tissues (thyroid, muscle, fat) had an averaged NIRAF signal-to-background ratio of 1.03 ± 0.02, which was significantly lower than both normal and diseased parathyroid glands ($p < 0.05$).

Of the 70 device measurements considered for data analysis, OTIS was able to enhance visualization at 67 of 70 regions of interest across 30 patients. Among these 3 tissue sites, 2 turned out to be PGs that had low NIRAF signal compared with the background and did not receive fluorescence projection overlay by OTIS. Measurements from the remaining one tissue site provided a noteworthy finding, as observed in patient 1 (see Table 1), where a suspect parathyroid candidate assessed with low confidence by the surgeon was imaged with OTIS. Because no NIRAF signal was detected, no green light was overlaid onto the tissue candidate. Subsequent frozen-section analysis confirmed that the specimen was composed of benign thyroid tissue only, highlighting the specificity of OTIS. Therefore, in terms of detection rate, OTIS managed to enhance visual contrast for 97% of PGs (67 of 69 PGs) directly in the surgical FOV without requiring any contrast agents.

DISCUSSION

In this article, we present a projection overlay system called OTIS that was designed to guide surgeons with improved visualization of PGs directly in the surgical field. The findings of this study demonstrated the applicability of OTIS for enhanced parathyroid visualization in an intraoperative setting. The results reveal that OTIS can detect 97% of parathyroid glands in vivo without requiring remote display monitors or exogenous contrast agents, highlighting OTIS as a novel tool that could potentially enhance parathyroid visualization directly within a surgeon's FOV. This system could eliminate erroneous image interpretation, supplement visual inspection, and potentially reduce surgical complications.

Reliable intraoperative localization of parathyroid glands, irrespective of disease state, could minimize patient morbidity by reducing incidences of postoperative hypocalcemia or repeat operations. Current clinical imaging modalities, such as sestamibi scintigraphy and ultrasound imaging, can only aid in preoperative localization of diseased parathyroid glands. Therefore, a surgeon typically relies on visual inspection to avoid damage/excision of healthy PGs or to

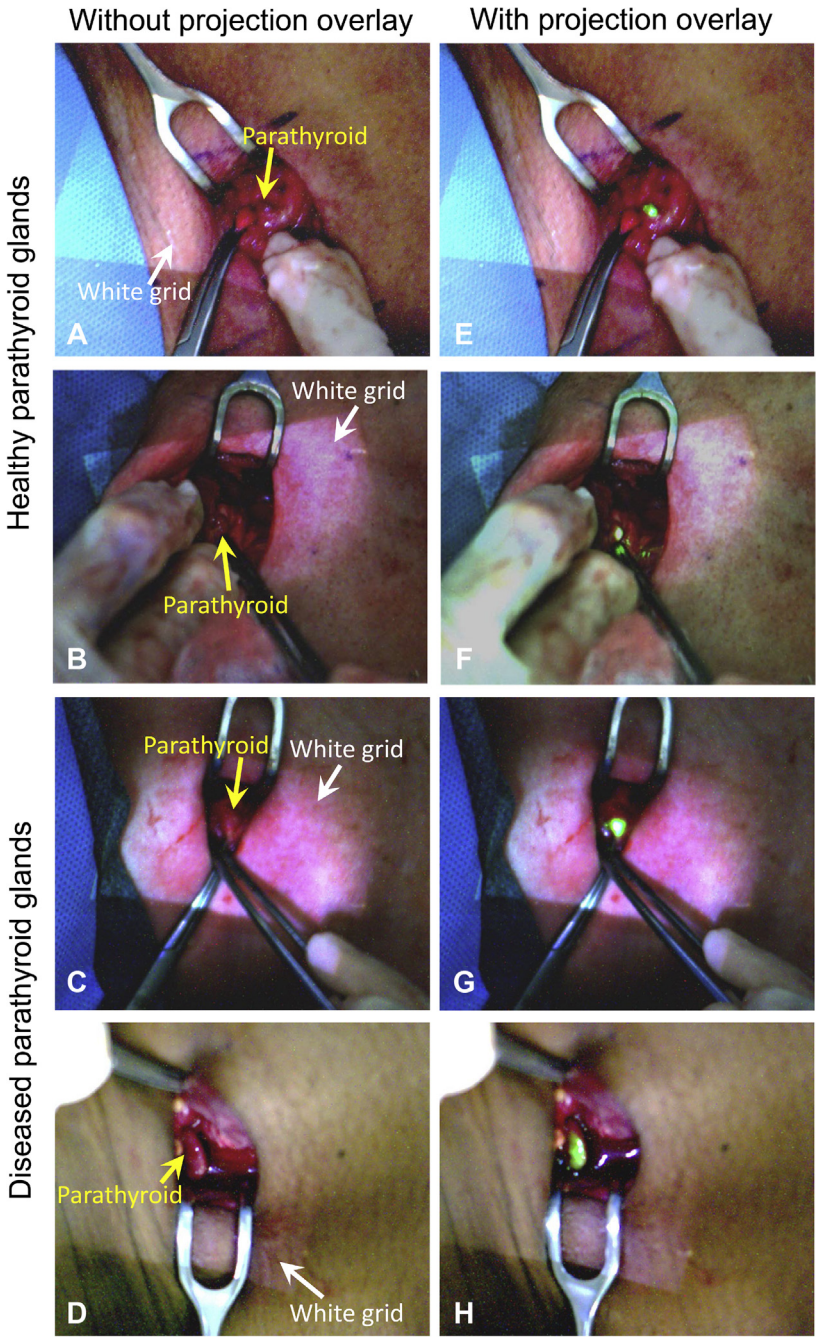

Figure 4. Intraoperative results with overlay tissue imaging system (OTIS) during thyroidectomies and parathyroidectomies. White light images of healthy parathyroid glands exposed in thyroidectomies for (A) benign multinodular goiter and (B) papillary thyroid carcinoma. White light images of diseased parathyroid glands—(C) parathyroid adenoma and (D) hyperplastic parathyroid gland from multiglandular hyperplasia—exposed during parathyroidectomies. (E–H) Corresponding images of the same regions as in Figure 4A to 4D with near infrared autofluorescence (NIRAF) projection overlay, where the parathyroid glands are overlaid with visible green light, enhancing its visibility to the surgeon's naked eye directly in the surgical field. Note that the other adjacent soft tissues in neck do not receive projection overlay due to weak NIRAF signal relative to parathyroid tissue. Parathyroid glands are indicated with yellow arrow in Figure. Rectangular white grid projection (indicated with white arrow) enables the surgeon to position the imaging-projection unit over region of interest.

ensure complete removal of diseased PGs in an intraoperative setting. The subjective nature of visual inspection and variability in surgical experience is a deterrent in correctly identifying PGs. This was the reason why discovery of NIRAF in PGs by Paras and colleagues[13] led to a rapid emergence of label-free NIRAF-based imaging modalities being considered for objectively guiding surgeons to accurate identification or localization of PGs.[14,17,20-22] However, these imaging systems typically depict grayscale NIRAF images on remote display monitors, which provides no spatial context of PGs in relation to adjacent structures. This might not be comparable with the actual surgical site and can lead to interpretive errors. In comparison, OTIS is distinct in projecting a processed image that highlights strong NIRAF regions, such as PGs directly onto the surgical FOV. Because PGs are visibly lit up directly within the surgical FOV, a more accurate spatial context of adjacent structures in relation to PGs can be observed without diverting the line of focus to a remote display monitor.

As seen in Figures 4A to 4D, it can be challenging for surgeons to distinguish PGs from their adjacent surroundings with the naked eye due to the homogeneous appearance of tissues in the surgical FOV. In stark contrast, image projection by OTIS in visible green light enhanced visibility for both healthy and diseased PGs (Figs. 4E to 4H). The visible contrast is further augmented because adjacent structures in the surgical FOV, such as thyroid gland, fat, and muscle, were not overlaid in green due to the relatively lower normal NIRAF intensity compared with PGs. In light of these findings, it must be highlighted that OTIS can project images within 0 to 1 mm accuracy, which yields a high degree of spatial precision, as evidenced in Figures 3A and 3C, at an imaging distance of 35 cm from the surgical FOV.[36] This was further validated with ex vivo tissue specimens (Figs. 3D, 3F), where only the 2 parathyroid adenomas were accurately overlaid in visible green, and the remaining tissues were not. Subsequently, Figure 4 demonstrated the intraoperative efficacy of OTIS in vivo enhancing visibility in 97% of PGs, distinguishing these from surrounding tissues.

It must, however, be considered that direct intraoperative visualization of PGs does not usually pose a major problem for experienced endocrine surgeons. This was clearly evident during data interpretation, as our surgeon correctly identified 66 of 70 (94.3%) tissues in neck with high confidence. We should also point out that our current study design involved a single surgeon who is highly experienced. Therefore, interpretation of benefits from a device such as OTIS would require a larger study design involving multiple surgeons with varied experience, skill sets, and patient volume because these parameters determine surgical outcomes eventually.[38-41] Nonetheless, accidental damage and devascularization of healthy PGs is a key challenge faced by even experienced surgeons, especially during radical neck operations that involve lymph node dissection. In such scenarios, OTIS can highlight healthy PGs directly in the surgical field, enabling surgeons to carefully maneuver dissection and avoid damage to PGs or its blood supply. Visualizing with OTIS can also be useful for scanning an excised thyroid specimen to look for healthy parathyroid tissue that might have been removed accidentally so that the surgeon can then autotransplant the parathyroid tissue back in the patient to prevent postoperative hypocalcemia. It must, however, be borne in mind that damage to PGs or their blood supply is a more common cause for postoperative hypocalcemia after thyroid operations, as accidental removal of healthy PGs is not as frequent. In such scenarios, surgeons would benefit from an objective modality that can evaluate parathyroid vascularity and/or viability as well, to minimize the risk of postoperative hypocalcemia. Although OTIS can aid the surgeon in being cautious when dissecting around healthy PGs, the technique by itself cannot provide insight about the vascularity or viability of the visualized PGs. In recent times, optical techniques, such as indocyanine green-based fluorescence angiography[42,43] or laser-speckle imaging[44] have demonstrated potential for assessing parathyroid perfusion or viability, and could therefore be used complementarily with NIRAF-based modalities such as OTIS.

With regard to detecting diseased/hyperfunctioning PGs, current imaging modalities typically use sestamibi scans to aid in preoperatively localizing adenomas, but this technique has a limited role in detecting multiglandular hyperplasia. Even then the gland location could shift during surgical dissection and might not match with preoperative scans. In such scenarios, OTIS can be used for intraoperatively identifying diseased PGs as depicted in Figures 4G and 4H. Because OTIS can visualize with a spatial resolution of 250 μm, it can detect PGs as small as 2 mm in diameter, which typically get missed using current methods. As a result, OTIS can prove useful for visualizing all types of PGs, and provide surgical guidance for ectopic glands and reoperative parathyroidectomies.

Although OTIS presents a novel feature of projecting the location of PGs directly within the surgical FOV, it must be noted that margins of the projected images did not precisely match those of parathyroid specimens because a 2-dimensional image is being projected onto a 3-dimensional structure. Despite this error, the current design parameters of OTIS suffice for simple parathyroid visualization, as the final overlay was capable of localizing PGs among other tissues ex vivo with 100% accuracy. This iterates that although OTIS performs optimally in

guiding surgeons to identify parathyroid tissue in his/her surgical FOV, the device should be optimized for operations that might require higher precision. When analyzing the performance of OTIS, it should be taken into account that all parathyroid candidates included in this study were exposed before measurement. The current system design of OTIS therefore allows confirmation of the identity of a suspect parathyroid candidate that is surgically exposed but might be limited in localizing a "missing" parathyroid. Although NIRAF signal can penetrate down to a few millimeters deep in soft tissue, it must be reemphasized that identifying/localizing PGs on the basis of NIRAF detection would additionally depend on the optical properties of tissues that lie above the suspect parathyroid candidate. In that respect, although it might be possible to visualize PGs below fatty layers, as demonstrated in the findings of Kim and colleagues,[21,45] the same principle will not be applicable for localizing deep-seated or intrathyroidal parathyroid glands, as the optical properties of thyroid tissues are significantly different from those of fatty layers. In addition, because the studies by Kim and colleagues did not precisely quantify the thickness of layers involved, additional studies will be required to investigate the depth-related detection limit of NIRAF signals from parathyroid using OTIS, which might aid in localizing PGs situated deeply. Although portability and flexibility of the OTIS setup can ensure a smooth transition into the surgical workflow, interference from ambient OR lights currently affects functionality of OTIS and other NIR imaging systems. It must be noted that data from 4 glands were excluded from the study because OR lights that remained on accidentally during those measurements masked NIRAF signal from the parathyroid candidates. This can, however, be addressed potentially in future iterations of OTIS by subtracting surgical OR light noise. Another aspect about the present system design of OTIS is that the motion of the image overlay is delayed in relation to that of the target by less than 2 seconds during dynamic projection. This time delay can be minimized further by using more rapid image processing algorithms in OTIS to ensure a more optimized dynamic image overlay projection. It should also be mentioned that the current user interface of OTIS would require additional simplification to ensure ease of use for the surgical personnel, akin to VeinViewer and Accuvein.[32,46] For this purpose, OTIS can be improved with a more intuitive user-interface in a manner similar to the PTeye—a user-friendly clinical prototype for label-free parathyroid identification—that was translated from the original research-grade system.[15] In terms of device safety, the current design of OTIS poses no risk to patients, as NIRAF from PGs can be visualized with an excitation power density of 0.6 mW/cm^2, which is lower than 11 mW/cm^2, which is reportedly used for parathyroid gland imaging with exogenous contrast.[47]

Because the surgeon remained blinded in our study design, it is currently unknown how OTIS could potentially affect patient outcomes. However, other modalities that have relied on NIRAF detection for localizing PGs like OTIS have presented promising preliminary results. Benmiloud and colleagues[20] recently demonstrated that using an NIR imaging system for parathyroid detection minimized postoperative hypocalcemia in thyroidectomies. The findings suggest that OTIS, in a manner similar to NIR imaging devices, could reduce these complications and improve patient outcomes. Another highlight of our study was the specificity of OTIS, which potentially allows exclusion of false-positive candidates assumed to be PGs. As described earlier, OTIS displayed no NIRAF signal for a tissue candidate identified by the surgeon as parathyroid adenoma that was eventually confirmed to be benign thyroid tissue. In that aspect, NIRAF-based modalities such as OTIS can be effective in reducing the number of frozen sections and related costs required for confirming PGs in real-time. This in turn could aid both surgeons and patients by minimizing the wait time of 20 minutes that is typically associated with frozen-section analysis, which again helps in cutting expenses associated with additional anesthesia administration.[48] The benefits of technology such as OTIS in hospitals and medical centers would, in turn, depend on the volume of operations done and the experience of the surgeon. In this regard, a device such as OTIS would mostly be valuable for early career surgeons with less experience at high-volume centers and established surgeons at low-volume centers, because surgeons with fewer years of experience or low-volume surgeons are associated with higher complication rates.[49-51] As with other surgical guidance devices, such as intraoperative nerve monitoring systems, a device like OTIS could also be a useful educative tool for training surgical residents in intraoperative parathyroid identification. In addition to label-free parathyroid visualization, OTIS can also be used in conjunction with suitable contrast agents for fluorescence image projection, which has potential for assessing tissue vascularity, tumor margin guidance, and sentinel lymph node detection, without requiring a display monitor.[33-36,42] These aspects render OTIS as a multifunctional device that could be considered a cost-effective investment for different type of operations by multiple surgeons. In terms of cost-effectiveness, once the use of a modality such as OTIS in the OR becomes more widespread, it would lead to mass production of similar devices, eventually resulting in affordable costs for the end-user. In terms of overall impact of this technology, future outcomes studies are necessary to investigate and assess whether OTIS,

alongside other NIRAF-based modalities, is valuable or not for a surgeon in terms of lowering the rates of post-surgical complications and related emergency department visits,[52] cutting health care expenditure,[53] and considerably limiting postoperative litigation.[54]

CONCLUSIONS

This article presents OTIS, a device that is capable of NIRAF-based image overlay directly onto the surgical field. Although the novelty and portability of OTIS can highly benefit surgeons in improving parathyroid visualization during head and neck operations, additional iterations of the device would allow OTIS to be seamlessly integrated into the current surgical workflow during thyroidectomies and parathyroidectomies. Success implementation of such a device is an innovative step toward enhancing visualization of PGs in real time without requiring display monitors or administering any exogenous labels.

Author Contributions

Study conception and design: McWade, Thomas, Nguyen, Sanders, Solórzano, Mahadevan-Jansen

Acquisition of data: McWade, Thomas, Nguyen, Solórzano

Analysis and interpretation of data: McWade, Thomas, Nguyen, Sanders, Mahadevan-Jansen

Drafting of manuscript: McWade, Thomas, Nguyen, Sanders, Solorzano, Mahadevan-Jansen

Critical revision: McWade, Thomas, Nguyen, Solorzano, Mahadevan-Jansen

Acknowledgment: We are grateful to the Vanderbilt University Medical Center hospital staff and surgical team involved for their assistance in data collection. We also thank Mr Adnan Abbas (AiBiomed) for his input on optimizing system design. The authors are also thankful to Emmanuel Mannoh and Christine O' Brien for their valuable guidance in preparing this manuscript.

REFERENCES

1. Bhattacharyya N, Fried MP. Assessment of the morbidity and complications of total thyroidectomy. Arch Otolaryngol 2002; 128:389–392.
2. Wells SA, Debenedetti MK, Doherty GM. Recurrent or persistent hyperparathyroidism. J Bone Miner Res 2002;17 [Suppl 2]:N158–M162.
3. Gourgiotis S, Moustafellos P, Dimopoulos N, et al. Inadvertent parathyroidectomy during thyroid surgery: the incidence of a complication of thyroidectomy. Langenbeck Arch 2006; 391:557–560.
4. Edafe O, Antakia R, Laskar N, et al. Systematic review and meta-analysis of predictors of post-thyroidectomy hypocalcaemia. Br J Surg 2014;101:307–320.
5. Caron NR, Sturgeon C, Clark OH. Persistent and recurrent hyperparathyroidism. Curr Treat Options Oncol 2004;5: 335–345.
6. Mohebati A, Shaha AR. Imaging techniques in parathyroid surgery for primary hyperparathyroidism. Am J Otolaryngol 2012;33:457–468.
7. Sukan A, Reyhan M, Aydin M, et al. Preoperative evaluation of hyperparathyroidism: the role of dual-phase parathyroid scintigraphy and ultrasound imaging. Ann Nucl Med 2008; 22:123–131.
8. Patel CN, Salahudeen HM, Lansdown M, Scarsbrook AF. Clinical utility of ultrasound and 99mTc sestamibi SPECT/CT for preoperative localization of parathyroid adenoma in patients with primary hyperparathyroidism. Clin Radiol 2010;65:278–287.
9. Chen H, Wang TS, Yen TW, et al. Operative failures after parathyroidectomy for hyperparathyroidism: the influence of surgical volume. Ann Surg 2010;252:691–695.
10. Reddy AC, Chand G, Sabaretnam M, et al. Prospective evaluation of intra-operative quick parathyroid hormone assay as an early predictor of post thyroidectomy hypocalcaemia. Int J Surg 2016;34:103–108.
11. Wilhelm SM, Wang TS, Ruan DT, et al. The American Association of Endocrine Surgeons Guidelines for Definitive Management of Primary Hyperparathyroidism. JAMA Surg 2016; 151:959–968.
12. Ahuja AT, Wong KT, Ching ASC, et al. Imaging for primary hyperparathyroidism—what beginners should know. Clin Radiol 2004;59:967–976.
13. Paras C, Keller M, White L, et al. Near-infrared autofluorescence for the detection of parathyroid glands. J Biomed Optics 2011;16:067012.
14. McWade MA, Sanders ME, Broome JT, et al. Establishing the clinical utility of autofluorescence spectroscopy for parathyroid detection. Surgery 2016;159:193–203.
15. Thomas G, McWade MA, Paras C, et al. Developing a clinical prototype to guide surgeons for intraoperative label-free identification of parathyroid glands in real time. Thyroid 2018;28: 1517–1531.
16. FDA. FDA permits marketing of two devices that detect parathyroid tissue in real-time during surgery. Available at: https://www.fda.gov/NewsEvents/Newsroom/PressAnnouncements/ucm624982.htm. Accessed November 3, 2018.
17. McWade MA, Paras C, White LM, et al. Label-free intraoperative parathyroid localization with near-infrared autofluorescence imaging. J Clin Endocrinol Metab 2014;99: 4574–4580.
18. Shinden Y, Nakajo A, Arima H, et al. Intraoperative identification of the parathyroid gland with a fluorescence detection system. World J Surg 2017;41:1506–1512.
19. Falco J, Dip F, Quadri P, et al. Increased identification of parathyroid glands using near infrared light during thyroid and parathyroid surgery. Surg Endosc 2017;31:3737–3742.
20. Benmiloud F, Rebaudet S, Varoquaux A, et al. Impact of autofluorescence-based identification of parathyroids during

total thyroidectomy on postoperative hypocalcemia: a before and after controlled study. Surgery 2018;163:23–30.
21. Kim SW, Song SH, Lee HS, et al. Intraoperative real-time localization of normal parathyroid glands with autofluorescence imaging. J Clin Endocrinol Metab 2016;101:4646–4652.
22. Ladurner R, Al Arabi N, Guendogar U, et al. Near-infrared autofluorescence imaging to detect parathyroid glands in thyroid surgery. Ann R Coll Surg Engl 2018;100:33–36.
23. Elliott JT, Dsouza AV, Davis SC, et al. Review of fluorescence guided surgery visualization and overlay techniques. Biomed Optics Express 2015;6:3765–3782.
24. Berguer R. Surgery and ergonomics. Arch Surg 1999;134:1011–1016.
25. Hanna GB, Shimi SM, Cuschieri A. Task performance in endoscopic surgery is influenced by location of the image display. Ann Surg 1998;227:481–484.
26. Krupinski EA. The role of perception in imaging: past and future. Semin Nucl Med 2011;41:392–400.
27. Krupinski EA. Current perspectives in medical image perception. Attent Percept Psychophys 2010;72:1205–1217.
28. Stone R, McCloy R. Ergonomics in medicine and surgery. BMJ 2004;328:1115–1118.
29. Killory BD, Nakaji P, Gonzales LF, et al. Prospective evaluation of surgical microscope-integrated intraoperative near-infrared indocyanine green angiography during cerebral arteriovenous malformation surgery. Neurosurgery 2009;65:456–462; discussion 462.
30. Watson JR, Gainer CF, Martirosyan N, et al. Augmented microscopy: real-time overlay of bright-field and near-infrared fluorescence images. J Biomed Optics 2015;20:106002.
31. Blackwell M, Nikou C, DiGioia AM, Kanade T. An image overlay system for medical data visualization. Med Image Anal 2000;4:67–72.
32. Juric S. Towards a low-cost mobile subcutaneous vein detection solution using near-infrared spectroscopy. Sci World J 2014;2014:365902.
33. Sarder P, Gullicksrud K, Mondal S, et al. Dynamic optical projection of acquired luminescence for aiding oncologic surgery. J Biomed Optics 2013;18:120501.
34. Ringhausen E, Wang T, Pitts J, et al. Evaluation of dynamic optical projection of acquired luminescence for sentinel lymph node biopsy in large animals. Technol Cancer Res Treat 2016;15:787–795.
35. Gan Q, Wang D, Ye J, et al. Benchtop and animal validation of a projective imaging system for potential use in intraoperative surgical guidance. PLoS One 2016;11:e0157794.
36. Nguyen JQM, McWade M, Thomas G, et al. Development of a modular fluorescence overlay tissue imaging system for wide-field intraoperative surgical guidance. J Med Imaging (Bellingham) 2018;5:021220.
37. Brunaud L, Zarnegar R, Wada N, et al. Incision length for standard thyroidectomy and parathyroidectomy: when is it minimally invasive? Arch Surg 2003;138:1140–1143.
38. Hauch A, Al-Qurayshi Z, Randolph G, Kandil E. The importance of surgical volume on outcomes in thyroid surgery revisited: old is in again. Ann Surg Oncol 2014;21:3721–3722.
39. Zarebczan B, Chen H. Influence of surgical volume on operative failures for hyperparathyroidism. Adv Surg 2011;45:237–248.
40. Sosa JA, Powe NR, Levine MA, et al. Thresholds for surgery and surgical outcomes for patients with primary hyperparathyroidism: a national survey of endocrine surgeons. J Clin Endocrinol Metab 1998;83:2658–2665.
41. Sosa JA, Bowman HM, Tielsch JM, et al. The importance of surgeon experience for clinical and economic outcomes from thyroidectomy. Ann Surg 1998;228:320–330.
42. Zaidi N, Bucak E, Yazici P, et al. The feasibility of indocyanine green fluorescence imaging for identifying and assessing the perfusion of parathyroid glands during total thyroidectomy. J Surg Oncol 2016;113:775–778.
43. Vidal Fortuny J, Belfontali V, Sadowski S, et al. Parathyroid gland angiography with indocyanine green fluorescence to predict parathyroid function after thyroid surgery. Br J Surg 2016;103:537–543.
44. Mannoh EA, Thomas G, Solórzano CC, Mahadevan-Jansen A. Intraoperative assessment of parathyroid viability using laser speckle contrast imaging. Sci Rep 2017;7:14798.
45. Kim SW, Lee HS, Ahn Y-C, et al. Near-infrared autofluorescence image-guided parathyroid gland mapping in thyroidectomy. J Am Coll Surg 2018;226:165–172.
46. Lamperti M, Pittiruti M. II. Difficult peripheral veins: turn on the lights. Br J Anaesth 2013;110:888–891.
47. Hyun H, Park MH, Owens EA, et al. Structure-inherent targeting of near-infrared fluorophores for parathyroid and thyroid gland imaging. Nat Med 2015;21:192–197.
48. Bollig CA, Gilley D, Lesko D, et al. Economic impact of frozen section for thyroid nodules with "suspicious for malignancy" cytology. Otolaryngol Head Neck Surg 2018;158:257–264.
49. Maruthappu M, Gilbert BJ, El-Harasis MA, et al. The influence of volume and experience on individual surgical performance: a systematic review. Ann Surg 2015;261:642–647.
50. Duclos A, Peix J-L, Colin C, et al. Influence of experience on performance of individual surgeons in thyroid surgery: prospective cross sectional multicentre study. BMJ 2012;344:d8041.
51. Toniato A, Boschin IM, Piotto A, et al. Complications in thyroid surgery for carcinoma: one institution's surgical experience. World J Surg 2008;32:572–575.
52. FitzGerald RA, Sehgal AR, Nichols JA, McHenry CR. Factors predictive of emergency department visits and hospitalization following thyroidectomy and parathyroidectomy. Ann Surg Oncol 2015;22[Suppl 3]:S707–S713.
53. Cote V, Sands N, Hier MP, et al. Cost savings associated with post-thyroidectomy parathyroid hormone levels. Otolaryngol Head Neck Surg 2008;138:204–208.
54. Ready AR, Barnes AD. Complications of thyroidectomy. Br J Surg 1994;81:1555–1556.